

Extracting Dynamical Models from Data

Michael F. Zimmer*

(Dated: September 30, 2022)

The problem of determining the underlying dynamics of a system when only given data of its state over time has challenged scientists for decades. In this paper, the approach of using machine learning to model the *updates* of the phase space variables is introduced; this is done as a function of the phase space variables. (More generally, the modeling is done over the jet space of the variables.) This approach is shown to accurately replicate the dynamics for the examples of the harmonic oscillator, the pendulum, and the Duffing oscillator; the underlying differential equation is also accurately recovered in each example. In addition, the results in no way depend on how the data is sampled over time (i.e., regularly or irregularly). It is demonstrated that this approach (named "FJet") is similar to the model resulting from a Taylor series expansion of the Runge-Kutta (RK) numerical integration scheme. This analogy confers the advantage of explicitly revealing the appropriate functions to use in the modeling, as well as revealing the error estimate for the updates. Thus, this new approach can be thought of as a way to determine the coefficients of an RK scheme by machine learning. Finally, it is shown in the undamped harmonic oscillator example that the stability of the updates is stable for 10^9 times longer than with 4th-order RK.

I. INTRODUCTION

Equations for dynamical systems have traditionally been derived by a variety of techniques of a theoretical, experimental, and/or intuitive nature. However, in the case that differential equations (DEs) are determined directly from a *data* source, perhaps with machine learning (ML) techniques, it is useful to identify the following subgoals:

1. Extrapolate model beyond training data times.
2. Determine underlying DE.
3. Determine parameter dependencies in DE.
4. Estimate stability/accuracy of model.
5. Determine related domain knowledge.

The present paper focuses on the first four points. The fifth point relates to conserved quantities and is discussed in detail in a companion paper (see earlier versions of [1] from Oct. 2021).

Background

Related developments in the field appear over the history of the subject, and are organized accordingly.

Classical : Systematically deriving DEs for dynamical systems can be identified as beginning with Newton's second law of motion [2]. Lagrange recast Newtonian mechanics, building on work of others to take into account constraints. Lagrangian mechanics are built in terms of the generalized coordinates and velocities (q, \dot{q}) , leading to the Euler-Lagrange equations. Hamilton gave the

modern version of the principle of least action, and after introducing a generalized momentum (p), and a Legendre transform (from $(q, \dot{q}) \rightarrow (q, p)$), produced the Hamiltonian mechanics. Non-conservative features may be accounted for by including Rayleigh dissipation, or by a generalization of Hamilton's variational principle [3].

Nonlinear Dynamics : The beginning of the study of nonlinear dynamics is widely identified with Poincaré's work [4, 5], owing to his studies on celestial mechanics, three-body problems, qualitative studies of nonlinear DEs [6], and a wealth of contributions for analyzing such systems (e.g., phase space, recurrence theorem, Poincaré-Bendixson theorem). Also, Lyapunov [7] studied the stability of ODEs, introducing an exponential characterization of the rate of growth of instabilities.

Chaos : Certain nonlinear systems may exhibit a sensitive dependence on initial conditions [8, 9], so that the long time difference between two states may become arbitrarily large (within the confines of the attractor), even though they were initially quite close. Such a phenomena was first studied by Lorenz [10] in the context of equations that modeled atmospheric convection. A general definition of chaos may be found in [Sec. 1.8 of 11].

The sensitive dependence on initial conditions can be measured by a Lyapunov exponent [8, 12], with a positive value signifying chaos [13]. In numerical simulations, there are thus two sources of instability: from discretization effects, and now from chaos [14]. The question of whether a solution of a chaotic system is even meaningful was answered in the affirmative with the *shadowing lemma* [15–19]. The length of time that a solution remains valid despite such instabilities was studied by [20].

Embeddings : In the context of fluid turbulence, there was interest in testing the Ruelle-Takens conjecture [21] concerning the role of a strange attractor. The challenge was to connect experimental time series data at a point to a strange attractor. It was shown by Packard et al. [22] that geometric aspects (i.e., Lyapunov exponent, topological dimension) of a Rössler model could be captured

* <http://www.neomath.com>

by using a lower dimensional manifold [23] and time-delay coordinates of a single scalar variable $s(t)$ (e.g., density, velocity component) at multiple times (cf. Sec 8.13 of [12]). Important related works include [24–26].

DE Models : A methodology for modeling the global dynamics was introduced by Crutchfield and McNamara [14]. The data was fit to a model of the form $dy/dt = F$, where the choice of F was guided by minimizing a complexity measure. They considered low-dimensional models, including the Lorenz model and the Duffing oscillator. A number of other significant works would soon follow, including [27–30], and others. In particular, [31, 32] would model the dynamics in the phase space, although in a manner different from the present work. The techniques that were used in this time period for modeling $F(y)$ included polynomial expansions, radial basis functions, neural nets (NNs), B-splines, Galerkin bases [33], etc; the reader is referred to the review by [34] for a more complete discussion.

Recent : There has been renewed attention to this problem, exploiting techniques from the ML community. A common theme has been to apply the time series data (from conserved dynamics) to an autoencoder, and to require that the latent variables (i.e., the middle layer) obey physical equations of motion, such as Hamilton’s equations [35–37] or the Euler-Lagrange equations [38, 39].

Another successful approach has been the application of symbolic dynamics, which uses a database of known functional forms; [40] have applied this to Graph NNs on a cosmology example. Also, symbolic regression has been improved using recursively exploited modularity [41]; it can detect generalized symmetries.

Software (SINDy) [42] has been used to search a specified function space while modeling, beginning with a regularized form of $dy/dt = F$; this was demonstrated on a number of ODEs and PDEs.

In addition, Neural ODEs [43–45] can replicate the dynamics of a system by first training a NN on data, and then using that NN for a new extrapolation. In this approach, each layer of the NN represents an update step in a numerical integration scheme for a DE.

Finally, there are other contributions besides these, but space does not permit a more complete review.

Other Related topics include time-series analysis, numerical integration, and Lie symmetries.

Time-Series Analysis: There is a long literature on time-series analysis [46], and there is significant overlap with what is being focused on here. The difference is that with a typical time-series analysis, there is little additional interest in finding the underlying dynamical equations that led to the data. Instead, the focus is often on finding a statistical characterization or perhaps on fitting a simple model. For this reason, no further discussion will be made of this.

Numerical Integration: At first glance it would seem that the topic of numerical integration [47–49] wouldn’t belong in this section. However, an expansion with respect to time of a scheme such as RK4 produces terms

that can reasonably be considered in a model. Thus it offers a principled means of determining the function space for the predictors of a model, and will be used throughout this paper.

Lie Symmetries: The present work will study the model with respect to small changes in the phase space variables, and sometimes higher derivatives. At the same time though, it is a goal of the larger effort to determine conserved quantities, such as energy or momentum. Lie symmetries were introduced to study invariances [50] of ODEs and PDEs, and will be considered in a companion paper for using the models computed herein to determine conserved quantities; this can be done even for non-conserved models.

Outline

The layout of the remainder of the paper is structured as follows. Section II introduces the FJet approach, going into detail in its Methodology subsection. In Sections III, IV and V are the three examples: Harmonic Oscillator, Pendulum, and Duffing Oscillator. The analysis in each of these sections follows a similar pattern: training data, model, underlying DE, extrapolation, etc. Section VI takes a larger view of how Runge-Kutta (RK) informs the choice of the function space to be used for X . Following that are the Final Remarks and several appendices. Appendix A analyzes the RK updates for each model, and shows how the function space of the predictor variables appear after a Taylor series expansion; these results play an important role in this paper. Appendix B collects results from the parameter fitting, and Appendix C displays plots of the residuals. Finally, Appendix D discusses a second optimization procedure which can improve the quality of a model

II. FJET APPROACH

The focus in this paper is on dynamical systems describable as an explicit n th-order ordinary DE (i.e., ODE)

$$u^{(n)} = G(t, u, u^{(1)}, \dots, u^{(n-1)}) \quad (1)$$

where $u^{(i)}$ represents the i th derivative of u with respect to t . Of course, the order of the equation won’t be known beforehand, nor will the form of G . Autonomous and non-autonomous cases will be considered herein.

As mentioned, the approach of related works has been to model u and $u^{(1)}$ as a function of t . Here the approach will be to model *changes* in $U^{(n-1)} = \{u, u^{(1)}, \dots, u^{(n-1)}\}$, known as the $(n-1)$ st prolongation [50] of $u(t)$. Specifically, for an n -dimensional system, the response variables are $Y = \Delta\mathcal{U}^{(n-1)} \equiv \{\Delta u, \Delta u^{(1)}, \dots, \Delta u^{(n-1)}\}$. For *autonomous* dynamics, the predictor variables are $X = \mathcal{U}^{(n-1)}$. For non-autonomous dynamics, the predictors are $X = Q \times$

$U^{(n-1)}$, otherwise known as the $(n-1)$ st jet space, where Q is the set of independent variables (in this case just $\{t\}$). For both cases (autonomous and non-autonomous), functions of the elements of X may be explicitly added to the set. Data for the variables in X and Y will be used to derive a model of the form $Y = h(X)$, where h generically represents the machine learning model. The FJet approach does *not* restrict the type of ML regression model used; for example, h may be a neural net (NN), a random forest, a boosting model, etc.

Methodology

There are several steps to the FJet approach, which are now discussed.

Step 1–*Create smooth fits to raw data.* The first step is taking the data provided on a system and putting it into a form usable by the FJet approach. Note that it isn't necessary to have the data appear as a time series; the times can be sampled randomly. Also, in order to obtain derivative information [51–53] a local fit to this data is first done, and derivatives are computed with respect to that. However, in the examples to be shown, the update and derivative information is derived from synthetic data, obviating this step.

Step 2–*Collect data for updates.* The second step is to use the smooth fits created in step #1 to obtain values for changes in u , \dot{u} over a fixed time step ϵ . In the case of a 2nd-order ODE, they are simply defined as

$$\Delta u = u(t + \epsilon) - u(t) \quad (2a)$$

$$\Delta \dot{u} = \dot{u}(t + \epsilon) - \dot{u}(t) \quad (2b)$$

At this point the data is in the form (X, Y) , which for a 2nd-order autonomous ODE would appear as $(u, \dot{u}, \Delta u, \Delta \dot{u})$ for each time t . Also, note that for an n th-order ODE, the set of response variables would include up to $\Delta u^{(n-1)}$.

Step 3–*Fit an ML model h .* The generic formula for modeling the system as $Y = h(X)$ must be specified for individual elements of Y . For the 2nd-order example it is written as $h = (h_1, h_2)$, which are defined as

$$\Delta u = h_1(u, \dot{u}) \quad (3a)$$

$$\Delta \dot{u} = h_2(u, \dot{u}) \quad (3b)$$

As mentioned previously, any suitable ML model may be used for h_1 or h_2 , such as NNs, random forest, boosting methods, etc. However, a particularly transparent and natural choice is something here named *feature regression*. It is written as

$$h = \alpha_1 f_1 + \alpha_2 f_2 + \dots \quad (4)$$

with scalars α_i and features f_i which are functions of the variables of X ; this can be thought of as an extension of polynomial regression. In the examples, f_i are typically monomials or may involve trigonometric functions. The

advantage this type of model offers is that it simplifies the interpretation of the model in terms of a DE when the time step $\epsilon \rightarrow 0$. Other authors refer to this as a *linear in the parameter model* [34].

Step 4–*Extrapolation.* Having obtained a model for the updates for a given time step ϵ , it is straightforward to use it to generate a time-sequence of values. This is done by the *generative algorithm* given in Algo. 1.

Algorithm 1 : Generative Algorithm: 2nd-order

```

Input:  $t_0, N$ 
Init:  $t = t_0$ 
Init:  $u = u(t)$ 
Init:  $\dot{u} = \dot{u}(t)$ 
for  $i = 0$  to  $N$  do
  tmp_h1 =  $h_1(u, \dot{u})$ 
  tmp_h2 =  $h_2(u, \dot{u})$ 
   $u \leftarrow u + \text{tmp\_}h_1$ 
   $\dot{u} \leftarrow \dot{u} + \text{tmp\_}h_2$ 
   $t \leftarrow t + \epsilon$ 
  print( $u, t$ )
end for

```

Note that as written, this algorithm applies to the 2nd-order example where $Y = \{\Delta u, \Delta \dot{u}\}$ and $X = \{u, \dot{u}\}$.

Step 5–*Refine the model.* Recall that the determination of the model h in Step #3 is based on a fit of the response (Y) variables as a function of the predictors (X). It is not based on how well the values for $u(t)$ it generates match those of the data. Thus, this presents an opportunity for a second optimization, in which the parameters obtained for h in Step #3 can be fine-tuned to better match the raw data. This is discussed in greater detail in Appendix D.

An additional step that can be taken to improve the results is to limit the domain of training data to only encompass the region of phase space where extrapolations are done. Doing otherwise will bias the model on unexplored regions, reducing the quality of the results in the domain of interest.

Step 6–*Estimating Stability/Accuracy.* The accuracy will be in part assessed through a comparison to the best solution available. In one instance this will be the exact solution; in the others it will be to an extrapolation using RK4. When available, comparisons will also be made to the energy of the system.

A limiting factor to the stability of the FJet solution is the completeness of the feature set. It is shown in Appendix A that the feature set is implied by an expansion of the Runge-Kutta numerical integration scheme, to a given order in the time step. This will be confirmed in the examples, where FJet achieves a level of accuracy of (at least) RK4 in one example, and a level of accuracy comparable to RK2 in the other two. In addition, a smaller value for ϵ of course leads to more accurate results.

Finally, the deviation of u , \dot{u} and parameter values measured with respect to their expected values, will be

evaluated with the function

$$\mathcal{E}_\sigma(p, p_{\text{ref}}) = \log_{10}|p - p_{\text{ref}}| \quad (5)$$

Here p is the value at hand (of u , \dot{u} or a parameter), p_{ref} is the reference value, and σ indicates the level of noise. This measure will be used throughout the paper.

Training Data

The training data is synthetic and will be generated by evolving the known, underlying DE forward in time by an amount ϵ ; this will be done for randomly chosen values of u and \dot{u} . The set of ϵ values to be used below will range from 0.001 to 0.1. To mitigate unnecessary discretization errors, the DE will be generated by a number of iterations of a time step $\epsilon_{\text{base}} = 0.001$. For example, to obtain data for a single instance of $(\Delta u, \Delta \dot{u})$ at $\epsilon = 0.1$, the RK4 scheme will be iterated 100 times using ϵ_{base} .

In addition, the bulk of the examples used training data that was made more realistic by including an additive *measurement error* of $\sigma\epsilon\nu$ to each entry of u and \dot{u}

$$\begin{aligned} u &\rightarrow u + \sigma\epsilon\nu \\ \dot{u} &\rightarrow \dot{u} + \sigma\epsilon\nu', \end{aligned}$$

where ν and ν' represent independent draws from a zero-mean, unit-variance normal distribution. Note that this also impacts functions of u and \dot{u} , as well as Δu and $\Delta \dot{u}$. The time step ϵ was included as a factor in the strength of ν to reflect that these measurements were made with respect to a smoothed fit of u , as discussed in Sec. II; a noise coefficient with constant strength would overwhelm Δu and $\Delta \dot{u}$ for small ϵ . Systematic deviations for u , \dot{u} that do not vanish as $\epsilon \rightarrow 0$ will not be considered. In this paper, the data will typically be modeled with $\sigma = 0$, 0.1 and 0.2.

III. EXAMPLE: HARMONIC OSCILLATOR

The equation for a harmonic oscillator is relevant for a myriad of physical systems, such as the small angle limit of a pendulum. Here, u represents the deviation from the minimum, ω_0 its natural frequency, and γ its damping coefficient

$$\ddot{u} + 2\gamma\dot{u} + \omega_0^2 u = 0. \quad (6)$$

The general solution in the underdamped case is $u(t) = Ae^{-\gamma t} \cos \omega t + Be^{-\gamma t} \sin \omega t$, where $\omega = \sqrt{\omega_0^2 - \gamma^2}$, and A and B are suitable coefficients. This section will consider this underdamped case unless stated otherwise.

Training Data

Training data was generated from 2000 random samples, using $\omega_0 = 1$, $\gamma = 0.1$, $T = 2\pi/\omega_0$, $t \in (0, 2T)$,

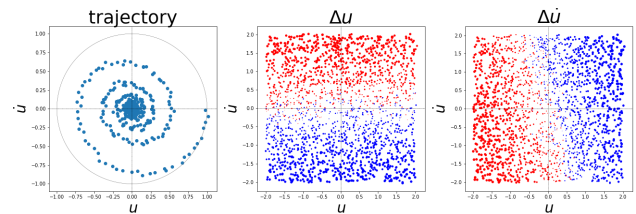


FIG. 1. Three plots for the harmonic oscillator, using a noise level of $\sigma = 0.2$. The left plot corresponds to the (clockwise) path taken by updates of the system, starting from an initial condition of $(u, \dot{u}) = (1, 0)$. The light gray circle is added as a visual reference, and corresponds to the path that would have been taken in the undamped, noiseless case. The center and right plots correspond to the changes in u and \dot{u} , as defined in Eq. 2.

$u \in (-2, 2)$, and $\dot{u} \in (-2, 2)$. In order to generate the Δu and $\Delta \dot{u}$, the data points were created with a time step $\epsilon = 0.1$ (with iterated updates of RK4) and $\sigma = 0.2$, as described near the end of Sec. II.

In the left plot of Fig. 1 a typical trajectory is shown using $\sigma = 0.2$, to show the impact of the noise. In both the center and right plots, the differences $(\Delta u, \Delta \dot{u})$ (computed between times t and $t + \epsilon$) are plotted with respect to the values at time t . In the plots, the color of the points is determined by the sign of Δu or $\Delta \dot{u}$: it is red (blue) if the sign is positive (negative). Also, the size of the dots is proportional to the magnitude of Δu (or $\Delta \dot{u}$); the same scaling was used for both plots in the figure. These figures provide useful information as to how to model Δu and $\Delta \dot{u}$ over this space. They demonstrate how to capture the dynamic information in static plots.

Model

Given these observations, it appears that it would suffice from a modeling perspective to simply have h_1 and h_2 be linear combinations of u and \dot{u} . However, following the guidance from Eq. A10, a large class of candidate features are initially considered.

$$\{u, \dot{u}\} \rightarrow \{u, \dot{u}, t, t^2, u^2, u\dot{u}, \dots\}.$$

It will be understood from Appendix A that several of these terms need not be considered (such as t , t^2) for dynamics with no explicit time dependence. (No constant term is expected, since it appears the dot size is zero near the origin, in both plots in Fig. 1. Also, note that if \ddot{u} were included in the predictors, a collinearity would manifest itself, a signal to the modeler that it should be removed.)

As already discussed, while many ML models can be used (such as a NN), it is convenient here to use *feature regression*, since it will later facilitate determining the underlying DE. From this set of candidate features, the usual techniques of regression [54] can be used to remove irrelevant predictors. The resulting response (Y)

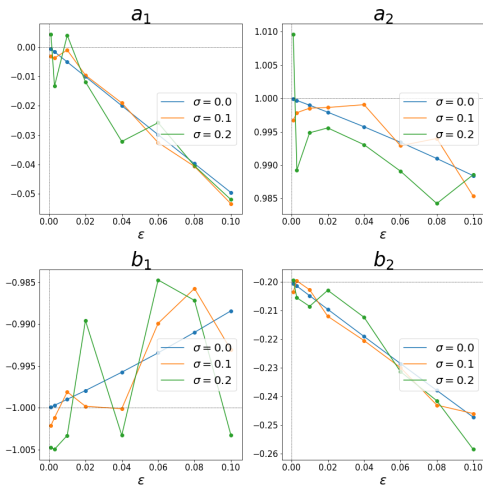


FIG. 2. Plots of the ϵ -dependence of the coefficients in the model $h(X)$ (cf. Eq. 9). The intersection of the thin vertical and horizontal gray lines indicate the correct value at $\epsilon = 0$. Note the different scales for the error for each plot.

and predictor (X) variables are chosen to be

$$Y = (\Delta u, \Delta \dot{u})^T \quad (7)$$

$$X = (u, \dot{u})^T, \quad (8)$$

and the feature regression model $Y = h(X)$ appears as a matrix-vector product

$$Y = \epsilon \begin{bmatrix} a_1 & a_2 \\ b_1 & b_2 \end{bmatrix} X. \quad (9)$$

In this approach, one can now determine the coefficients a_i and b_i ($i = 1, 2$) by fitting it to the training data using $\epsilon = 0.1$. Note that an explicit regularization was not used, in contrast to approaches by other authors [eg. 14, 42]. With regularization, one might have used, for example, elastic net regularization [54] to drive small, less important coefficients down to zero. Instead, it will be shown next that creating a feature regression model for *several* values of ϵ , with *no* regularization, can also lead to a controlled derivation of the underlying DE.

Underlying DE

The process of fitting Y to X for a single ϵ is now repeated for the set of ϵ -values $\{0.001, \dots, 0.1\}$, leading to the plots in Fig. 2; these plots include data for the cases $\sigma = 0, 0.1$, and 0.2 . Best line fits were used to model the ϵ -dependence, with the results collected in Table V in Appendix B. These fits were extrapolated to $\epsilon = 0$ to determine parameter values for the underlying DE. Equation 9 may now be rewritten in this limiting case, and the variables will be written using the standard differential notation (i.e., $\epsilon \rightarrow dt$, $\Delta u \rightarrow du$, $\Delta \dot{u} \rightarrow d\dot{u}$),

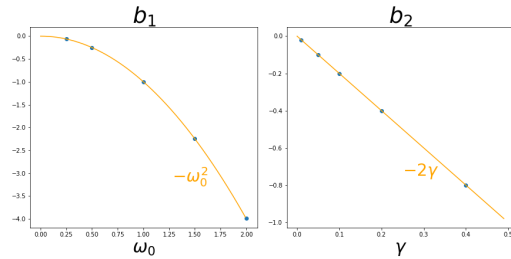


FIG. 3. The dependence of b_1 and b_2 as a function of ω_0 and γ is plotted using blue dots. As a visual guide, the exact curves for $-\omega_0^2$ and -2γ are added as orange curves to the left and right plots, respectively.

producing

$$du = dt [\dot{u}] \quad (10a)$$

$$d\dot{u} = dt [-0.2\dot{u} - u] \quad (10b)$$

(Of course, this is a slight abuse of notation, since derivatives are defined in a limiting procedure.) The first of these equations (Eq. 10a) is just a contact condition, and reflects the fact that in the space (u, \dot{u}) , not all three quantities du , dt , \dot{u} are independent (i.e., $\dot{u} = du/dt$). When these two equations are combined, they are just equivalent to the original equation of motion for the damped harmonic oscillator (Eq. 6), with the chosen parameter values ($\omega_0 = 1$ and $\gamma = 0.1$).

A. Parameter Dependence

What was obtained in the previous section is the equation of motion based on the choice $\omega_0 = 1$, $\gamma = 0.1$. In this section, the actual functional dependence on ω_0 and γ within the equation of motion is deduced.

The idea here is to consider a given value of ϵ , and several values of ω_0 . This produces a plot versus ω_0 , which is then fit with a low-order polynomial in ω_0 . Thus, the fitting parameters are now determined for that one, given value of ϵ . Next, this procedure is repeated for several other small values of ϵ , and the result is extrapolated to $\epsilon = 0$. In this section the fitting was done for the zero noise case (i.e., $\sigma = 0$), and led to the results: $b_1 = -\omega_0^2 + \dots$, $b_2 = -2\gamma + \dots$. Shown in Fig. 3 is the ω_0 and γ dependence for these parameters in the specific case of $\epsilon = 0.001$. From this, Eq. 10a and Eq. 10b can be replaced with

$$du = dt [\dot{u}] \quad (11)$$

$$d\dot{u} = dt [-2\gamma\dot{u} - \omega_0^2 u] \quad (12)$$

from which the original equation of motion (Eq. 6) immediately follows. In summary, it has been shown how to obtain the complete equation of motion (along with parameter dependence), from data.

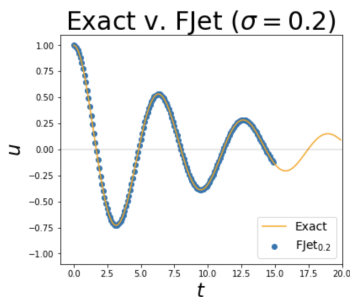


FIG. 4. A comparison of the extrapolation of the exact solution to that generated by FJet with $\sigma = 0.2$.

Extrapolation & Stability

There are three approaches for this example in which the stability and the extrapolation accuracy of the FJet models will be evaluated.

First Approach: One may do an extrapolation in time using the model parameter values for FJet with $\sigma = 0.2$, and do a visual comparison. Upon using the generative algorithm with $\epsilon = 0.1$, Fig. 4 results. Thus for these shorter times, close agreement is visually confirmed. However, for longer times such a graph is less informative, and so the next approach is considered.

Second Approach: A way to understand the extrapolation accuracy is to compare it to the exact solution mentioned earlier. The error measure defined in Eq. 5 is used in Fig. 5 to compare the magnitudes of the errors for the solutions found using RK and FJet; included in the plot are the results from an optimized solution (using Appendix D). What is most noticeable in the $\sigma = 0$ plot is the small error of FJet₀ compared to RK2 and the optimized solution; note the log scale.

Third Approach: A way to compare the accuracy of extrapolations is to compute the energy in the undamped case: $E = \frac{1}{2}(u^2 + \dot{u}^2)$, where now $\omega_0 = 1$ and $\gamma = 0$. Following [55], the energy at the n th iteration (E_n) is parametrized as exponentially changing

$$E_n/E_0 = \exp(\lambda n) \quad (13)$$

Thus, a λ closer to 0 means it is more stable. Iterating for 10^4 iterations, with the initial condition of $(u, \dot{u}) = (1, 0)$, led to the values in Table I. The most obvious aspect to this table is the much smaller value of λ for FJet₀

TABLE I. In the case where $\gamma = 0$ (undamped), and $\sigma = 0$ (zero noise), FJet (using feature regression) remains stable about 10^9 times longer than RK4.

scheme	λ
Euler	9.94×10^{-2}
RK2	2.49×10^{-5}
RK4	-1.38×10^{-8}
FJet ₀	-1.63×10^{-17}

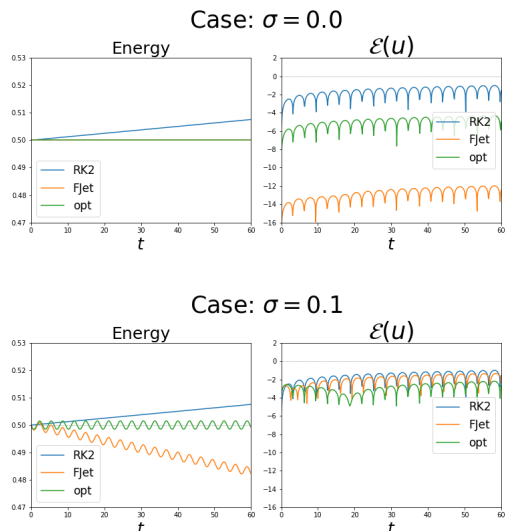


FIG. 5. For $\sigma = 0$, the energy values for *opt* overlaps that of FJet, and neither has any discernable deviation from the exact value of 0.5. Also, for this case note the much lower error values for FJet on this log scale; the optimization process (Appendix D) reduces the accuracy from this nearly ideal case. For the case $\sigma = 0.1$, the *opt* solution fares better than FJet or RK2.

(with feature regression); it means that FJet₀ remains stable for about 10^9 times longer compared to RK4. The parameter values used for FJet₀ were computed using $\epsilon = 0.1$ and appear in Table. II, along with comparison values from Euler/RK2/RK4.

IV. EXAMPLE: PENDULUM

The equation of motion for the damped pendulum is

$$\ddot{u} + 2\gamma\dot{u} + \omega_0^2 \sin u = 0 \quad (14)$$

where ω_0 is the natural frequency in the small- u limit and γ is the damping coefficient.

Training Data

The parameter values $\omega_0 = 1.0$ and $\gamma = 0.1$ are used in Fig. 6, which includes multi-start trajectories (left plot),

TABLE II. Parameter values for the *undamped* harmonic oscillator with $\gamma = 0$ and $\epsilon = 0.1$. The third column "FJet₀" refers to the zero-noise case, and was found using feature regression.

	Euler	RK2	RK4	FJet ₀
a_1	0	-0.005	-0.004995833	-0.004995834721974124
a_2	0.1	0.1	0.099833	0.09983341664682731

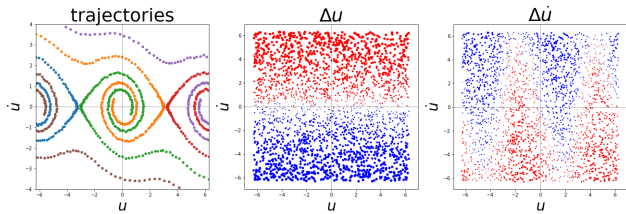


FIG. 6. Three plots for the pendulum, using a noise level of $\sigma = 0.2$. The left plot displays multiple trajectories, starting from a number of different initial conditions. Note the 2π periodicity along u . The center and right plots correspond to the changes in u and \dot{u} , as defined in Eq. 2.

and the update maps Δu and $\Delta \dot{u}$ (center and right plots). Note that in the left plot, the rotation is clockwise; in the upper (lower) half of the plane, the motion is to the right (left). The Δ -plots were created by randomly selecting 2000 (u, \dot{u}) values and then doing a single time step update with RK4 (with iterated updates), using $\epsilon = 0.1$. The three plots in this figure have u and \dot{u} each range over $(-2\pi, 2\pi)$ to display the periodic structure, but in the actual training data only the range of $(-\pi, \pi)$ was used. This created a data pair, and allowed a creation of data for Δu and $\Delta \dot{u}$. It is these plots which will be fitted by an ML procedure. As before, the dot sizes are proportional to the magnitude of what is being plotted; they are colored red (blue) for positive (negative) values.

Model

As a starting assumption, based on experience with a harmonic oscillator, one might begin by considering the feature set $\{u, \dot{u}\}$. However, the domain knowledge in this case is that u must be periodic, so instead the starting feature set under consideration is $\{\dot{u}, \cos u, \sin u\}$. As discussed in Appendix A, numerical integration techniques suggest one should use a larger feature set, such as

$$\{\dot{u}, \cos u, \sin u\} \rightarrow \{\dot{u}, \cos u, \sin u, \dot{u} \cos u, \dot{u} \sin u, \dots\}$$

The elements in this new set may now be taken as input features into an appropriate ML model. As already discussed, while many ML models can be used (such as NNs), it is convenient here to use *feature regression*, since it will facilitate determining the underlying DE. After following the usual steps in regression [54], the resulting response (Y) and predictor (X) variables are chosen to be

$$Y = (\Delta u, \Delta \dot{u})^T \quad (15a)$$

$$X = (\dot{u}, \sin u, \dot{u} \cos u)^T \quad (15b)$$

and the feature regression model $h(X)$ appears as a matrix-vector product,

$$Y = \epsilon \begin{bmatrix} a_1 & a_2 & a_3 \\ b_1 & b_2 & b_3 \end{bmatrix} X \quad (16)$$

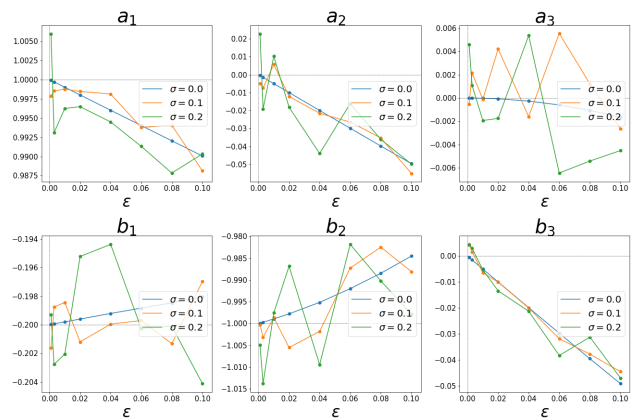


FIG. 7. Plots of the ϵ -dependence of the coefficients in the model $h(X)$ (cf. Eq. 16). The intersection of the thin vertical and horizontal gray lines indicate the correct value at $\epsilon = 0$.

In this approach, one can now determine the coefficients a_i and b_i ($i = 1, 2, 3$) by fitting it to the training data using $\epsilon = 0.1$. (Note that validation and test data could be used for a refined approach.) In the feature regression modeling, regularization was not used, in contrast to approaches by other authors [eg. 14, 42].

Underlying DE

The process of fitting Y to X for a single ϵ is now repeated for the set of ϵ -values $\{0.001, \dots, 0.1\}$, leading to the plots in Fig. 7; these plots include data for the cases $\sigma = 0$, $\sigma = 0.1$ and $\sigma = 0.2$. Best line fits were used to model the ϵ -dependence, with the results collected in Table V in Appendix B. These fits were extrapolated to $\epsilon \rightarrow 0$ to determine parameter values for the underlying DE. Equation 16 may now be rewritten in this limiting case, and the variables will be written using the standard differential notation (i.e., $\epsilon \rightarrow dt$, $\Delta u \rightarrow du$, $\Delta \dot{u} \rightarrow d\dot{u}$), producing

$$du = dt[\dot{u}] \quad (17a)$$

$$d\dot{u} = dt[-0.2\dot{u} - \sin u] \quad (17b)$$

The first of these equations (Eq. 17a) is just a contact condition, and reflects the fact that in the space (u, \dot{u}) , not all three quantities du , dt , \dot{u} are independent (i.e., $\dot{u} = du/dt$). The combination of these two equations is just equivalent to the original equation of motion for the pendulum (Eq. 14), with the chosen parameter values.

Extrapolation & Stability

Using $\epsilon = 0.1$ and the values for a_i and b_i found earlier, an extrapolation of $u(t)$ can be created using Algo. 1 along with initial conditions $(u, \dot{u}) = (1, 0)$. This is performed for the undamped case ($\gamma = 0$), so that the energy

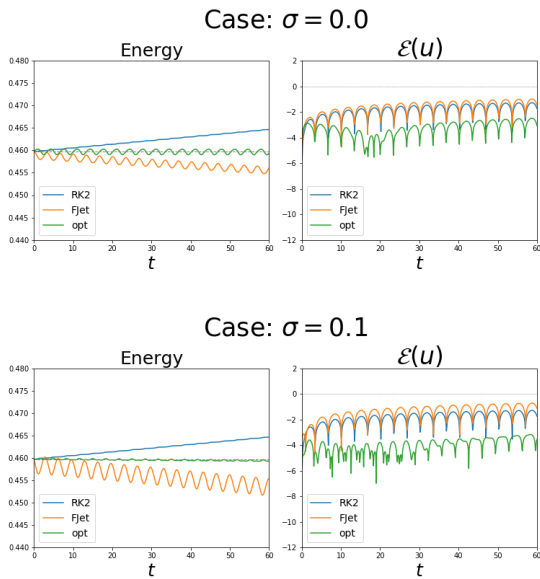


FIG. 8. The errors in energy for RK2 and FJet are comparable. The *opt* solution fares better than FJet or RK2, for either noise level. Since the initial condition is $(u, \dot{u}) = (1, 0)$, the energy is $1 - \cos(1) \approx 0.46$.

(E), as defined by

$$E = \frac{1}{2} \dot{u}^2 + \omega_0^2 (1 - \cos u), \quad (18)$$

can also be examined to see if it remains conserved. Shown in Fig. 8 are plots of the energy and the error (as defined in Eq. 5). The data are from RK2, FJet, and the optimized FJet; this is for the cases of $\sigma = 0$ and 0.1. As can be seen, the plots reveal that FJet and RK2 perform comparably, while the optimized version of FJet performs much better.

V. EXAMPLE: DUFFING OSCILLATOR

The Duffing oscillator [8, 56–59] is similar to the damped oscillator seen in Sec. III, except it allows for a nonlinear restoring force and an external force $p(t)$. It appears here as

$$\ddot{u} + 2\gamma\dot{u} + \alpha u + \beta u^3 = p(t) \quad (19a)$$

$$p(t) = A \cos \Omega t \quad (19b)$$

Training Data

This example used the parameter values $\gamma = 0.15$, $\alpha = -1$, $\beta = 1$, $A = 0.28$, and $\Omega = 1.2$, resulting in the plots of Fig. 9. The left plot was created from a

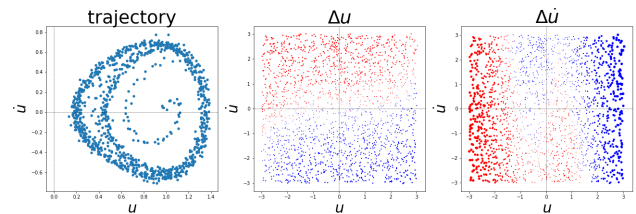


FIG. 9. Three plots for the Duffing oscillator, using a noise level of $\sigma = 0.2$. The left plot corresponds to the (clockwise) path taken by updates of the system, starting from an initial condition of $(u, \dot{u}) = (1, 0)$. The center and right plots correspond to the changes in u and \dot{u} , as defined in Eq. 2. Also, note the different scale of the left plot compared to the others.

single run with initial condition $(u, \dot{u}) = (1, 0)$; the updates lead to a clockwise rotation. Note that the orbit displays a period-2 oscillation (cf. pp453-462 in [59], and [57]), and that it has only positive u -values (since the α and β values create a double-well potential). The center and right plots are the update maps Δu and $\Delta \dot{u}$. As before, the dot sizes are proportional to the magnitude of what is being plotted, and are red (blue) for positive (negative) values. The training data was obtained by randomly sampling 2000 points; the sampling domain for u , \dot{u} and t were $(-3, 3)$, $(-3, 3)$, and $(0, 4\pi/\Omega)$, respectively. As before, the second point was created by doing a single time-step update (with $\epsilon = 0.1$) using RK4 with iterated updates. The random time was inserted into Eq. 19b to create sampling for p and \dot{p} . This created a data pair, and allowed a creation of Δu and $\Delta \dot{u}$. Note that the plots for Δu and $\Delta \dot{u}$ do not include the independent variables p and \dot{p} (or time). Because of this, Fig. 9 is a plot that has a collapsed domain from (u, \dot{u}, p, \dot{p}) to (u, \dot{u}) , and thus there is a slight overlap of red and blue dots, even for $\sigma = 0$. (Of course, the presence of noise (i.e., $\sigma \neq 0$) also leads to a mixing of the red and blue dots.) Finally, it is noted that to create data that will lead to models that better support extrapolations with different $p(t)$ (e.g., different values for A or Ω), it could be advantageous to also sample over a range of A and Ω .

Model

While a starting assumption for the feature set might be $\{u, \dot{u}, p\}$, the discussion of Runge-Kutta in Appendix A suggests it should be enlarged, such as

$$\{u, \dot{u}, p\} \rightarrow \{u, \dot{u}, u^2, u\dot{u}, \dot{u}^2, u^3, u^2\dot{u}, u\dot{u}^2, \dot{u}^3, p, \dot{p}, pu, p\dot{u}, \dot{p}u, \dot{p}\dot{u}, \dots\} \quad (20)$$

The elements in this new set may now be taken as input features into an appropriate ML model. As already discussed, while many ML models can be used (such as a NN), it is convenient here to use *feature regression*, since it will facilitate determining the underlying DE. After following the usual steps in regression [54] the resulting

response (Y) and predictor (X) variables are chosen to be

$$Y = (\Delta u, \Delta \dot{u})^T \quad (21)$$

$$X = (u, \dot{u}, u^3, u^2 \dot{u}, u \dot{u}^2, \dot{u}^3, p, \dot{p})^T \quad (22)$$

In Appendix A, it is shown how a RK expansion motivates which terms should be included, and the terms $u \dot{u}^2$ and \dot{u}^3 were not amongst them. However, here they were included to demonstrate that the technique is resilient against the addition of unnecessary terms. The feature regression model $Y = h(X)$ appears as a matrix-vector product,

$$Y = \epsilon \begin{bmatrix} a_1 & a_2 & a_3 & 0 & 0 & 0 & a_7 & 0 \\ b_1 & b_2 & b_3 & b_4 & b_5 & b_6 & b_7 & b_8 \end{bmatrix} X. \quad (23)$$

In this approach, one can now determine the coefficients a_i and b_i ($i = 1, \dots, 8$) by fitting it to the training data; a_4, a_5, a_6, a_8 were already identified as being essentially 0. Note that the resulting FJet mapping can then make use of any forcing term in an extrapolation algorithm; all that is needed is knowledge of p and \dot{p} at a series of times. Because of its reliance on a general p (and \dot{p}), it resembles a Green's function approach.

In the feature regression modeling, regularization was not used, in contrast to approaches by other authors [eg. 14, 42]. For example, one might have used regularization to drive small, less important coefficients down to zero, enabling an easier identification of a "minimal model". Instead, the ϵ -dependence of these parameters will be studied in the next sub-section, to determine their behavior as $\epsilon \rightarrow 0$ and ascertain the underlying DE.

A model for the Duffing equation was also reconstructed from phase space data by [60], where they included two first-order equations for $p(t)$ to model its oscillatory dynamics. In doing so, they were able to study the Duffing oscillator as an autonomous system with four first-order ODEs.

Underlying DE

The process of fitting Y to X for a single ϵ is now repeated for the set of ϵ -values $\{0.001, \dots, 0.1\}$, leading to the plots in Figs. 10, 11; these plots include data for the cases $\sigma = 0, 0.1, \text{ and } 0.2$. Best line fits were used to model the ϵ -dependence, with the results collected in Table V in Appendix B; in three of the cases it was appropriate to use polynomial regression up to second-order. These fits were extrapolated to $\epsilon \rightarrow 0$ to determine parameter values for the underlying DE. Equation 23 may now be rewritten in this limiting case, and the variables will be written using the standard differential notation (i.e., $\epsilon \rightarrow dt$, $\Delta u \rightarrow du$, $\Delta \dot{u} \rightarrow d\dot{u}$), producing

$$du = dt [\dot{u}] \quad (24a)$$

$$d\dot{u} = dt [-0.3\dot{u} + u - u^3 + p] \quad (24b)$$

The first of these equations (Eq. 24a) is just a contact condition, and reflects the fact that in the space (u, \dot{u}) , not all three quantities du , dt , \dot{u} are independent (i.e., $\dot{u} = du/dt$). The combination of these two equations is just equivalent to the original equation of motion for the Duffing oscillator (Eq. 19), with the chosen parameter values.

Extrapolation

Using $\epsilon = 0.1$ and the values for a_i and b_i found earlier, an extrapolation of $u(t)$ can be created using an extension of the earlier generative algorithm, here shown as Algo. 2.

Algorithm 2 : Generation step for Duffing oscillator

```

Input:  $t_0, N, \{p\}, \{\dot{p}\}$ 
Init:  $t = t_0$ 
Init:  $u = u(t_0)$ 
Init:  $\dot{u} = \dot{u}(t_0)$ 
for  $i = 0$  to  $N$  do
  tmp_h1 =  $h_1(u, \dot{u}, p(t), \dot{p}(t))$ 
  tmp_h2 =  $h_2(u, \dot{u}, p(t), \dot{p}(t))$ 
   $u \leftarrow u + \text{tmp}_h1$ 
   $\dot{u} \leftarrow \dot{u} + \text{tmp}_h2$ 
   $t \leftarrow t + \epsilon$ 
  print( $u, t$ )
end for

```

This extension is made because during training the values of p and \dot{p} are recorded (as scalars), and are included in the feature set X for training. Thus, during extrapolation, new values for p and \dot{p} are fed into this algorithm. (The notation $\{p\}, \{\dot{p}\}$ is used to denote that *functions* for p, \dot{p} are being passed in to this algorithm, and are evaluated at time t .) In principle any smooth function can be used for $p(t)$, but for the sake of numerical accuracy, it should be well approximated by its Taylor series expansion for small time steps.

Shown in Fig. 12 are plots of the error with respect to RK4 (using Eq. 5) for the cases $\sigma = 0$ and 0.1, with initial condition $(u, \dot{u}) = (1, 0)$. The data are from RK2, FJet, and the optimized FJet. In this case, FJet performs comparably to RK2 when there is no noise, but slightly worse when noise is present. In both cases, the optimized version of FJet performs at least as well as RK2, in general.

VI. SPACE OF FUNCTIONS FOR $h(X)$

In one sense, the present work is similar to the works reviewed in Sec. I, which used an expansion of low-order polynomials or simple functions as an approximation of the dynamics. However, in this paper it has been shown that there is a precise set of functions that should be used, based on a comparison to a Taylor series expansion of the corresponding Runge-Kutta scheme. This was possible

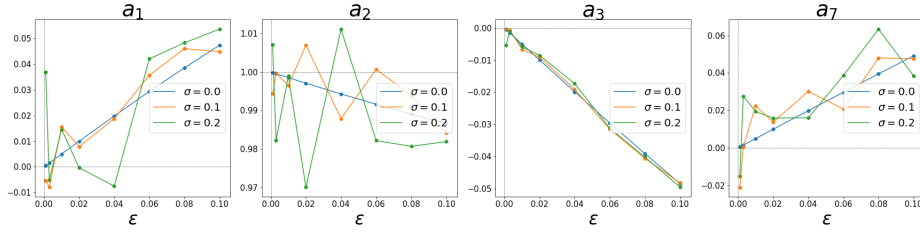


FIG. 10. Plots of the ϵ -dependence of the a_i coefficients ($i = 1, 2, 3, 7$) in the model $h(X)$ (cf. Eq. 23). The intersection of the thin vertical and horizontal gray lines indicate the correct value at $\epsilon = 0$.

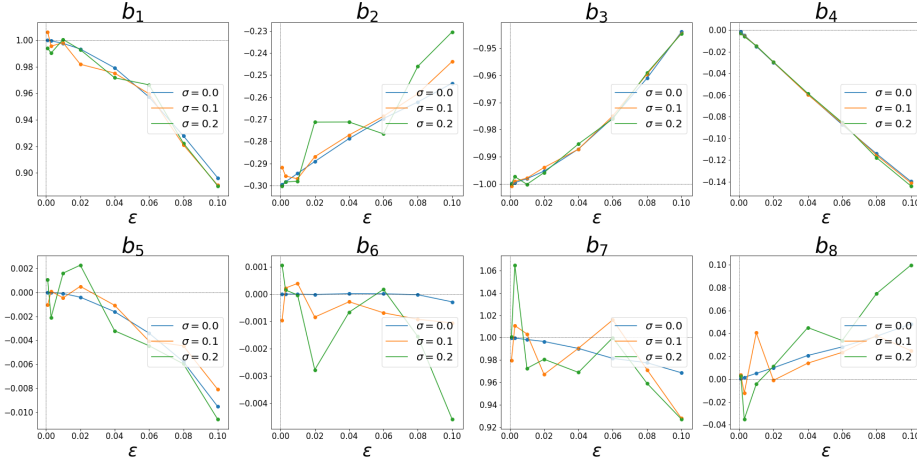


FIG. 11. Plots of the ϵ -dependence of the b_i coefficients ($i = 1, \dots, 8$) in the model $h(X)$ (cf. Eq. 23). The intersection of the thin vertical and horizontal gray lines indicate the correct value at $\epsilon = 0$.

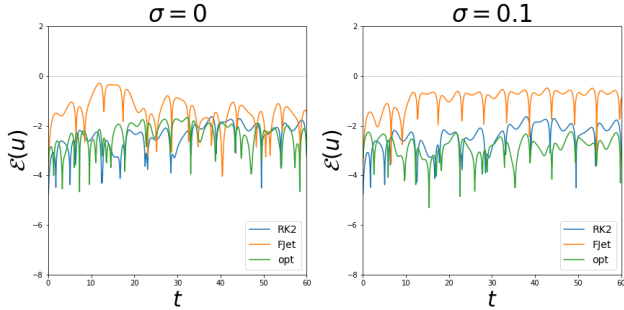


FIG. 12. Here the *opt* solution and RK2 are comparable. In this case the FJet solution fares slightly worse.

because this paper takes the unique position of modeling the dynamics using dependent variables from the jet space (i.e., the phase space in the examples studied).

In this section, define X_n as the set of features (or functions) needed to achieve $O(\epsilon^n)$ accuracy, as derived from a Taylor series expansion of the RK scheme. Such sets were derived implicitly for all three examples in Appendix A. In Table III, the sets are explicitly identified for the pendulum example. Understanding the origin of the features in this way is instructive: given a new data set for a physical system, a simpler system with a known DE can be studied to determine the kinds of features

that result, and those can then be considered for use in modeling. For example, if one wished to study the Duffing oscillator with multiplicative coupling of the forcing term $p(t)$ and u , then the approach here would indicate how to modify the feature set X . Another pathway for exploiting this insight is to first use candidate functions for X , derive an underlying DE, and then from that DE perform an expansion on the corresponding RK scheme to see if the resulting functions (i.e., X_n) are the same as the candidate functions; they should be.

Finally, note that for the two nonlinear examples studied here (i.e., pendulum and Duffing oscillator), $X_n \subset X_{n+1}$, while for the linear example (i.e., harmonic oscillator), X_n is a fixed set, independent of n .

TABLE III. The required feature set X_n for the pendulum example to achieve accuracy $O(\epsilon^n)$ in an RK context. It is shown for $n = 2$ (Euler), $n = 3$ (RK2), and $n = 5$ (RK4). Observe that $X_n \subset X_{n+1}$.

n	X_n
2	$\{\dot{u}, \sin u\}$
3	$\{\dot{u}, \sin u, \dot{u} \cos u\}$
5	$\{\dot{u}, \sin u, \dot{u} \cos u, \dot{u}^2 \sin u, \sin u \cos u, \dot{u}^3 \cos u, \dot{u} \sin^2 u, \dot{u} \cos^2 u\}$

VII. FINAL REMARKS

The FJet method has been introduced as an alternative means to model dynamical data and produce the underlying DE. It does so by performing ML modeling on updates in the phase space of the system. More generally it is $U^{(n-1)}$, when the underlying equation is of order n . In the FJet approach, the update data is formed by storing differences in the phase space variables over a small time step. In contrast, competing methods typically perform modeling over the time domain (cf. Sec. I).

The FJet approach can be understood from the vantage point of the numerical integration scheme Runge-Kutta. By expanding an RK scheme with respect to the time step (ϵ), certain features automatically appear. These features can be identified as the appropriate functions to use in a feature regression for a given example; this was demonstrated for all three examples. In particular, in the Duffing oscillator example (cf. Eq. 23), the identified features included terms for an external time-dependent force, in analogy to a Green's function approach. Finally, these considerations led to a general recommendation (Eq. A10) for what features to include, in the normal experimental scenario where the equation of motion isn't known beforehand.

While the modeling in this paper was done exclusively using feature regression, one should not make the mistake of thinking that it is a requirement. As pointed out at several points in the paper, any regression technique may be used. The reason for using feature regression is that it facilitates determining the underlying DE. If that is not a goal of the researcher, then other ML methods (such as NNs, XG-Boost, Random Forests) become competitive options.

In the three examples considered, it was demonstrated how the FJet model could lead to extrapolations beyond the range of the original training data. The accuracy of this extrapolation depends upon the number of variables, as well as the quality of the initial data for the updates (i.e., Δu , $\Delta \dot{u}$). In general, it was seen that if the feature set X included all the features from RK2 (after it was Taylor series expanded, as in Appendix A), then it could be expected to be at least as accurate as RK2. The same can be said with respect to RK4. However, in the case where X happens to be the exact feature set, as may happen in linear problems, then it is possible to obtain an extremely accurate solution, one that is accurate up to machine precision. Such was the case with the harmonic oscillator example.

The initial features that are considered herein are relatively complex (e.g., $\dot{u} \sin u$ in the Pendulum example) compared to other models, which commonly use a simple polynomial in u , for example. It is here asserted by the author that there is an interplay between the complexity of the initial features, and the complexity of the remaining ML model. In particular, it is asserted that for models of comparable (predictive) quality, the sum of these two complexities is approximately constant. The

author advocates for models with relatively complex initial features, as they make it easier to train and easier to understand the model, whether the remaining model be relatively simple (regression) or complex (NNs). Also, the initial features are a good place for the researcher to incorporate any subject matter expertise (e.g., with respect to heuristics, constraints, symmetries, or physical laws). Finally, it was seen in the examples that complex initial features simplify the determination of the underlying DE.

Other researchers have similarly determined the underlying DE for a dynamical model. However, to the best of the author's understanding, they proceeded by performing a fitting for a small time step, while including a regularization term. In contrast, the approach taken here was not to use regularization, and instead perform several fits at different time steps, and then extrapolate the various coefficients to their value at vanishing time step (i.e., $\epsilon \rightarrow 0$). In the present work, excellent agreement was seen via such an extrapolation.

ACKNOWLEDGEMENT

The author found general inspiration for considering this subject from attending the Kavli Institute for Theoretical Physics conference *At the Crossroads of Physics and Machine Learning*, Santa Barbara, Feb 2019. Also, the author kindly acknowledges the insightful instruction on differential equations and dynamical systems from Prof. Julian I. Palmore and Prof. E. Atlee Jackson (d.) at U. Illinois at Urbana-Champaign during the author's studies there.

Appendix A: Runge-Kutta

The Runge-Kutta scheme [47, 48] is a standard technique for the numerical integration of a solution given its ODE. An n th-order explicit ODE can be rewritten as a system of first-order DEs, and thus the general form for the ODE can be expressed as

$$\frac{dy}{dt} = f(t, y) \quad (\text{A1})$$

where $t(y)$ represents the independent (dependent) variables. The RK scheme involves an update from y_n to y_{n+1} , where the difference is

$$\Delta y_n \equiv y_{n+1} - y_n \quad (\text{A2})$$

After defining these quantities

$$k_1 = \epsilon f(t_n, y_n) \quad (\text{A3})$$

$$k_2 = \epsilon f\left(t_n + \frac{1}{2}\epsilon, y_n + \frac{1}{2}k_1\right) \quad (\text{A4})$$

$$k_3 = \epsilon f\left(t_n + \frac{1}{2}\epsilon, y_n + \frac{1}{2}k_2\right) \quad (\text{A5})$$

$$k_4 = \epsilon f(t_n + \epsilon, y_n + k_3) \quad (\text{A6})$$

the schemes for Euler, RK2 and RK4 can be summarized in Table IV. Note how complexity is built up in this scheme. For nonlinear ODEs this can lead to many terms involving powers and derivatives of the original variables.

In the subsections to follow, Δy will be computed in the RK2 scheme and then expanded with respect to ϵ ; importantly, this expansion is done to the same order in ϵ as the original RK expression. Since FJet are models of Δy , this expansion essentially becomes a derivation of the models $h = (h_1, h_2, \dots)$ in the feature regression technique. In the examples to follow, $y = (u, \dot{u})$, and so

$$\Delta y = \begin{bmatrix} \Delta u \\ \Delta \dot{u} \end{bmatrix} = \begin{bmatrix} h_1 \\ h_2 \end{bmatrix}$$

where h_1 and h_2 are functions of (u, \dot{u}) . Also, throughout this appendix, the substitution $v = \dot{u}$ will be used.

Harmonic Oscillator

The equation for the damped harmonic oscillator (Eq. 6) can be written as

$$\begin{bmatrix} \dot{u} \\ \dot{v} \end{bmatrix} = \begin{bmatrix} v \\ -\omega_0^2 u - 2\gamma v \end{bmatrix} = f \left(\begin{bmatrix} u \\ v \end{bmatrix} \right)$$

Note that there is no explicit time dependence in f . The RK2 scheme produces

$$\begin{aligned} \begin{bmatrix} h_1 \\ h_2 \end{bmatrix} &= \epsilon \begin{bmatrix} v - \frac{\epsilon}{2}\omega_0^2 u - \epsilon\gamma v \\ -\omega_0^2(u + \frac{\epsilon}{2}v) - 2\gamma(v - \frac{\epsilon}{2}\omega_0^2 u - \epsilon\gamma v) \end{bmatrix} \\ &= \epsilon \begin{bmatrix} -\frac{\epsilon}{2}\omega_0^2 & 1 - \epsilon\gamma \\ -\omega_0^2(1 - \epsilon\gamma) & -2\gamma(1 - \epsilon\gamma) - \frac{\epsilon}{2}\omega_0^2 \end{bmatrix} \begin{bmatrix} u \\ v \end{bmatrix} \end{aligned} \quad (\text{A7a})$$

$$\begin{aligned} \begin{bmatrix} h_1 \\ h_2 \end{bmatrix} &= \epsilon \begin{bmatrix} (1 - \epsilon\gamma)v - \frac{\epsilon}{2}\omega_0^2 \sin u \\ -2\gamma(1 - \epsilon\gamma)v + \epsilon\gamma\omega_0^2 \sin u - \omega_0^2 \sin(u + \frac{\epsilon}{2}v) \end{bmatrix} \\ &= \epsilon \begin{bmatrix} (1 - \epsilon\gamma) & -\frac{\epsilon}{2}\omega_0^2 & 0 \\ -2\gamma(1 - \epsilon\gamma) & -\omega_0^2(1 - \epsilon\gamma) & -\frac{\epsilon}{2}\omega_0^2 \end{bmatrix} \begin{bmatrix} v \\ \sin u \\ v \cos u \end{bmatrix} + O(\epsilon^3) \end{aligned} \quad (\text{A8a})$$

Observe that since this is being compared to RK2, a difference of $O(\epsilon^3)$ in Eq. A8a is irrelevant.

Thus, this expansion in ϵ produces a model akin to the feature regression technique, with the set of predictor variables: $\{v, \sin u, v \cos u\}$. If the RK4 were instead used, the reader would find this set to be

$$\{v, \sin u, v \cos u, v^2 \sin u, \sin u \cos u, v^3 \cos u, v \sin^2 u\}$$

Note how these extra terms could arise from Eq. A10.

This shows the how the vector $(u, v)^T$ naturally appears as the features. Since this is a linear differential equation, the same set of features results for RK4. Using the same definitions of a_1, a_2, b_1, b_2 as in Eq. 9, the RK4 results

TABLE IV. Update values Δy_n for three numerical integration schemes. Note the different level of accuracy in the time step ϵ .

Scheme	Δy_n	Accuracy
Euler	k_1	$O(\epsilon^2)$
RK2	k_2	$O(\epsilon^3)$
RK4	$\frac{1}{6}(k_1 + 2k_2 + 2k_3 + k_4)$	$O(\epsilon^5)$

are

$$\begin{aligned} a_1 &= -\frac{\epsilon}{6}\omega_0^2 \left(3 - 2\epsilon\gamma + \epsilon^2\gamma^2 - \frac{1}{4}\epsilon^2\omega_0^2 \right) \\ a_2 &= \frac{1}{6} \left(6 - 6\epsilon\gamma + 4\epsilon^2\gamma^2 - 2\epsilon^3\gamma^3 - \epsilon^2\omega_0^2 + \epsilon^3\gamma\omega_0^2 \right) \\ b_1 &= -\frac{1}{6}\omega_0^2 \left(6 - 6\epsilon\gamma + 4\epsilon^2\gamma^2 - 2\epsilon^3\gamma^3 - \epsilon^2\omega_0^2 + \epsilon^3\gamma\omega_0^2 \right) \\ b_2 &= \frac{1}{6} \left(-12\gamma + 12\epsilon\gamma^2 - 8\epsilon^2\gamma^3 + 4\epsilon^3\gamma^4 - 3\epsilon\omega_0^2 \right. \\ &\quad \left. + \frac{\epsilon^3}{4}\omega_0^4 + 4\epsilon^2\gamma\omega_0^2 - 3\epsilon^3\gamma^2\omega_0^2 \right) \end{aligned}$$

Pendulum

Equation 14 can be rewritten as

$$\begin{bmatrix} \dot{u} \\ \dot{v} \end{bmatrix} = \begin{bmatrix} v \\ -2\gamma\dot{u} - \omega_0^2 \sin u \end{bmatrix} = f \left(\begin{bmatrix} u \\ v \end{bmatrix} \right)$$

Note that there is no explicit time dependence in f . The RK2 scheme produces Eq. A8a

Duffing Oscillator

Equation 19 can be rewritten as

$$\begin{bmatrix} \dot{u} \\ \dot{v} \end{bmatrix} = f \left(t, \begin{bmatrix} u \\ v \end{bmatrix} \right) = \begin{bmatrix} v \\ -2\gamma v - \alpha u - \beta u^3 + p(t) \end{bmatrix}$$

Note that in this case there is explicit time dependence in f due to $p(t)$. The RK2 scheme produces Eq. A9a

$$\begin{aligned}
\begin{bmatrix} h_1 \\ h_2 \end{bmatrix} &= \epsilon \begin{bmatrix} (1 - \epsilon\gamma)v - \frac{\epsilon}{2}\alpha u - \frac{\epsilon}{2}\beta u^3 + \frac{\epsilon}{2}p(t) \\ -2\gamma(1 - \epsilon\gamma)v - \frac{\epsilon}{2}\alpha v - \alpha(1 - \epsilon\gamma)u + \epsilon\beta\gamma u^3 - \beta(u + \frac{\epsilon}{2}v)^3 - \epsilon\gamma p(t) + p(t + \frac{\epsilon}{2}) \end{bmatrix} \\
&= \epsilon \begin{bmatrix} -\frac{\epsilon}{2}\alpha & (1 - \epsilon\gamma) & -\frac{\epsilon}{2}\beta & 0 & \frac{\epsilon}{2} & 0 \\ -\alpha(1 - \epsilon\gamma) & -2\gamma(1 - \epsilon\gamma) - \frac{\epsilon}{2}\alpha & -\beta(1 - \epsilon\gamma) & -\frac{3\epsilon}{2}\beta & (1 - \epsilon\gamma) & \frac{\epsilon}{2} \end{bmatrix} \begin{bmatrix} u \\ v \\ u^3 \\ u^2v \\ p \\ \dot{p} \end{bmatrix} + \mathcal{O}(\epsilon^3) \quad (\text{A9a})
\end{aligned}$$

where \dot{p} denotes the time derivative of p . Once again, the $\mathcal{O}(\epsilon^3)$ expansion is an equivalent rewriting, since this is for RK2. Thus, this numerical integration scheme implies the vector of predictor variables $X = (v, u, u^3, u^2v, p, \dot{p})^T$ if feature regression is used.

General Expansion

Consider the above cases, where there is no explicit time dependence. In that case, the k_i can be written

$$k_{i+1} = \epsilon f \left(\begin{bmatrix} u + \delta u_i \\ v + \delta v_i \end{bmatrix} \right)$$

where $i = 1, 2, 3$ and k_1 is just ϵf . Now use subscripts a, b to identify the top (a) and bottom (b) components of the 2-by-1 vector:

$$\begin{aligned}
\delta u_1 &= (1, 0) \begin{bmatrix} \frac{1}{2}k_1 \\ \frac{1}{2}k_1 \end{bmatrix} \equiv (\frac{1}{2}k_1)_a = \frac{\epsilon}{2}f_a \\
\delta v_1 &= (0, 1) \begin{bmatrix} \frac{1}{2}k_1 \\ \frac{1}{2}k_1 \end{bmatrix} \equiv (\frac{1}{2}k_1)_b = \frac{\epsilon}{2}f_b
\end{aligned}$$

Likewise,

$$\begin{aligned}
\delta u_2 &= (\frac{1}{2}k_2)_a \\
\delta v_2 &= (\frac{1}{2}k_2)_b \\
\delta u_3 &= (k_3)_a \\
\delta v_3 &= (k_3)_b
\end{aligned}$$

Using the expression for k_{i+1} and expanding it with respect to δu_i and δv_i , and taking advantage of the fact that (e.g., in the case of the damped pendulum) many of the mixed partial derivatives of f with respect to u and v are zero, one obtains

$$\begin{aligned}
k_{i+1} &= \epsilon \{ f + \delta u_i \partial_u f + \delta v_i \partial_v f + \frac{1}{2!} (\delta u_i)^2 \partial_u^2 f \\
&\quad + \frac{1}{3!} (\delta u_i)^3 \partial_u^3 f + \dots \}
\end{aligned}$$

where $\partial_u f = \partial f / \partial u$, etc. This expansion is stopped at third order, because higher orders will lead to contributions beginning at $\mathcal{O}(\epsilon^5)$. These are ignored for the case

of RK4 since it is an $\mathcal{O}(\epsilon^5)$ algorithm. The point of doing this expansion is to demonstrate how low complexity models might be motivated from the standpoint of a numerical integration scheme. The above equation shows that all manner of monomials result, involving the original feature set and various derivatives and products of them. Also, keep in mind that the complexity builds on this, since k_1 gets substituted into k_2 , and then into k_3 and k_4 .

It is the previous expression for k_{i+1} which is used to motivate the following rubric, and is meant as a guide for which terms to include in the model. If \mathcal{F} is the original set of features, then the full set of *potential* features that should be considered are

$$\mathcal{F} \rightarrow \sum_{n=1} (\mathcal{F} + \partial_J \mathcal{F} + \partial_J \partial_J \mathcal{F} + \dots)^n \quad (\text{A10})$$

where ∂_J includes all possible partial derivatives and J denotes any of the jet space variables being used. (For example, in the harmonic oscillator and pendulum examples, $J = \{u, \dot{u}\}$; for the Duffing oscillator $J = \{t, u, \dot{u}\}$. However, the time derivative would only be applied to variables with an explicit time dependence, such as $p(t)$, but not u or \dot{u} .) If there are any special symmetry considerations, that should also be included. One should keep in mind that this rubric produces a *superset* of the terms that would result from a Runge-Kutta expansion. The extent to which every possible combination actually appears depends on the amount of nonlinearity in the underlying DE. In particular, linear problems like the harmonic oscillator have no contributions beyond \mathcal{F} (ignoring constant terms).

Appendix B: Parameter Fitting

As shown in Table V, the linear extrapolations between RK2 and FJet (for $\sigma = 0, 0.1$) agree well. The differences between the values at $\epsilon = 0$ lead to the errors in Table VI. The errors when $\sigma = 0$ are small, but as expected they increase slightly for increasing σ .

Appendix C: Residuals

In this section, plots are made of the residuals for each example using the FJet and RK models. The residuals are calculated as

$$\text{res}(u) = h_1 - \Delta u \quad (\text{C1a})$$

$$\text{res}(\dot{u}) = h_2 - \Delta \dot{u} \quad (\text{C1b})$$

where as before, $(\Delta u, \Delta \dot{u})$ are the data, and (h_1, h_2) are the predictions. For FJet, h_1 and h_2 are the derived models (cf. Eq. 3); for RK2, they are the Taylor-expanded versions of the usual RK2 (cf. Eqs. A7a,A8a,A9a). Note that here the residual is defined as "predicted - data", since the sampled data is taken as the ground truth. (This is a minor point, but residuals are usually defined as "data - predicted".) Also, as before, the red (blue) dots indicate positive (negative) values, with the size of the dot being proportional to its magnitude. Note that such plots are only conceivable for the FJet approach, and not the other approaches mentioned in Sec. I.

Regions of predominantly blue or red dots are indicate systematic deviations of the model from the data. It may be due to a poor fit, or that there aren't enough terms in the feature set X (i.e., a bias due to insufficient complexity in X). Also, the maximum magnitudes of the

TABLE V. Linear fits for each parameter as a function of the time step ϵ . The three sections, from top to bottom, correspond to the harmonic oscillator, the pendulum, and the Duffing oscillator. The values expected from RK2 (cf. Appendix A) are in the second column; the third and fourth columns contain the fits from FJet for the cases of $\sigma = 0$ and $\sigma = 0.2$. A quadratic fit in ϵ was used for b_1 , b_3 , and b_5 in the Duffing example.

	RK2	FJet ₀	FJet _{0.2}
a_1	$0 - 0.5\epsilon$	$-0.000 - 0.496\epsilon$	$-0.001 - 0.507\epsilon$
a_2	$1 - 0.1\epsilon$	$1.000 - 0.115\epsilon$	$0.998 - 0.134\epsilon$
b_1	$-1 + 0.1\epsilon$	$-1.000 + 0.115\epsilon$	$-1.001 + 0.092\epsilon$
b_2	$-0.2 - 0.48\epsilon$	$-0.200 - 0.473\epsilon$	$-0.198 - 0.555\epsilon$
a_1	$1 - 0.1\epsilon$	$1.000 - 0.099\epsilon$	$0.999 - 0.109\epsilon$
a_2	$0 - 0.5\epsilon$	$-0.000 - 0.496\epsilon$	$0.001 - 0.509\epsilon$
a_3	$0 + 0\epsilon$	$0.000 - 0.016\epsilon$	$0.002 - 0.077\epsilon$
b_1	$-0.2 + 0.02\epsilon$	$-0.200 + 0.019\epsilon$	$-0.199 - 0.022\epsilon$
b_2	$-1 + 0.1\epsilon$	$-1.001 + 0.152\epsilon$	$-1.003 + 0.129\epsilon$
b_3	$0 - 0.5\epsilon$	$-0.000 - 0.492\epsilon$	$0.001 - 0.490\epsilon$
a_1	$0 + 0.5\epsilon$	$0.000 + 0.475\epsilon$	$0.005 + 0.454\epsilon$
a_2	$1 - 0.15\epsilon$	$1.000 - 0.134\epsilon$	$0.994 - 0.129\epsilon$
a_3	$0 - 0.5\epsilon$	$-0.000 - 0.486\epsilon$	$-0.001 - 0.483\epsilon$
a_7	$0 + 0.5\epsilon$	$0.000 + 0.491\epsilon$	$0.008 + 0.453\epsilon$
b_1	$1 - 0.15\epsilon$	$1.000 - 0.224\epsilon$	$0.994 + 0.070\epsilon$
b_2	$-0.3 + 0.545\epsilon$	$-0.299 + 0.465\epsilon$	$-0.299 + 0.642\epsilon$
b_3	$-1 + 0.15\epsilon$	$-1.000 + 0.172\epsilon$	$-1.000 + 0.202\epsilon$
b_4	$0 - 1.5\epsilon$	$-0.001 - 1.407\epsilon$	$-0.001 - 1.435\epsilon$
b_5	$0 + 0\epsilon$	$-0.000 + 0.001\epsilon$	$0.001 - 0.015\epsilon$
b_6	$0 + 0\epsilon$	$0.000 - 0.002\epsilon$	$0.000 - 0.034\epsilon$
b_7	$1 - 0.15\epsilon$	$1.001 - 0.314\epsilon$	$1.014 - 0.748\epsilon$
b_8	$0 + 0.5\epsilon$	$0.000 + 0.475\epsilon$	$-0.015 + 1.117\epsilon$

residuals for each plot are summarized in Table VII; all values in that table are multiplied by 10^4 .

In each of the three examples, the figures were derived using the FJet model obtained when $\sigma = 0$; for the Duffing example, the $\sigma = 0.1$ case was also included. For the harmonic oscillator example shown in Fig. 13, the most noteworthy feature for the FJet model is the seemingly random placement of red and blue dots, which indicate no systematic residual. As revealed in Table VII, the scale for the dots is extremely small, on the order of 10^{-15} (i.e., machine precision in this case). These two facts are indicative of an excellent fit by FJet using feature regression. In contrast, the RK2 residuals display systematic deviation, with dot sizes on a scale about 10^{11} times larger.

The residuals for the pendulum example in Fig. 14 show systematic deviation for both FJet and RK2, and is likely due to the limited feature set used in modeling. Higher order features are suggested in Appendix A. As shown in Table VII, the residuals are smaller for FJet.

For the Duffing example, there are also systematic deviations seen in Fig. 15. As with the Pendulum example, these are likely due to a limited feature set. Fig. 16 is also displayed, to show how when noise is present ($\sigma = 0.1$) it can largely overwhelms the systematic deviations, leaving mostly randomly placed red and blue dots.

TABLE VI. Errors for the $\epsilon = 0$ extrapolation of the FJet model of the harmonic oscillator for the cases of $\sigma = 0, 0.1, 0.2$. The error is measured by Eq. 5. The three sections, from top to bottom, correspond to the harmonic oscillator, the pendulum, and the Duffing oscillator.

	\mathcal{E}_0	$\mathcal{E}_{0.1}$	$\mathcal{E}_{0.2}$
a_1	-4.43	-3.58	-3.02
a_2	-3.81	-3.25	-2.77
b_1	-3.81	-2.86	-2.91
b_2	-4.17	-3.23	-2.75
a_1	-5.19	-3.34	-2.90
a_2	-4.31	-3.54	-2.91
a_3	-3.79	-2.81	-2.73
b_1	-5.37	-3.56	-2.97
b_2	-3.27	-2.46	-2.54
b_3	-4.05	-2.98	-3.22
a_1	-3.50	-2.80	-2.31
a_2	-3.81	-3.33	-2.25
a_3	-3.76	-4.04	-3.05
a_7	-4.01	-3.41	-2.11
b_1	-3.31	-3.59	-2.25
b_2	-3.00	-2.58	-3.11
b_3	-3.89	-3.48	-3.62
b_4	-2.93	-2.84	-3.03
b_5	-4.58	-3.50	-3.26
b_6	-4.48	-3.73	-3.53
b_7	-2.86	-3.27	-1.87
b_8	-3.58	-2.26	-1.81

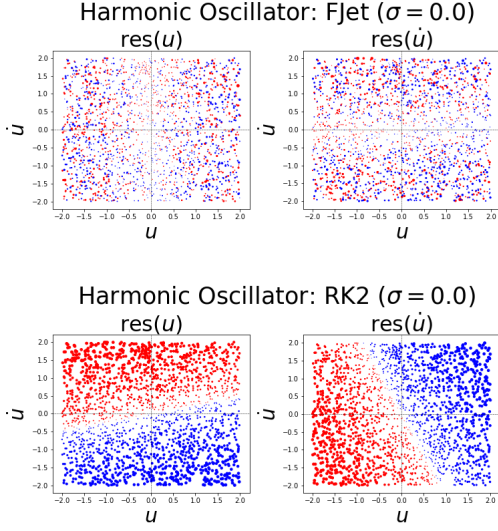


FIG. 13. Residuals for the harmonic oscillator example for the FJet model (top) and RK2 (bottom). The left and right plots are computed according to Eq. C1. The magnitude of the largest dots are given in Table VII.

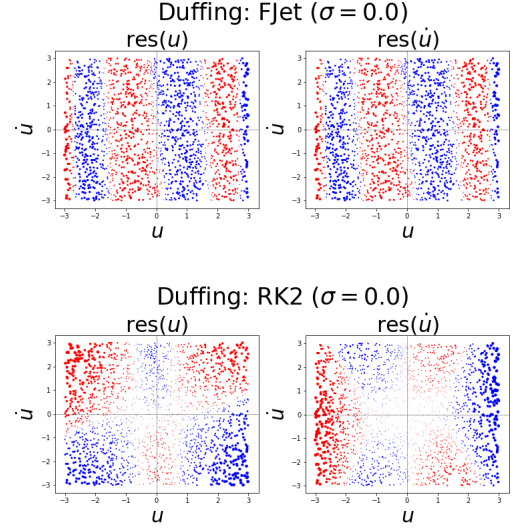


FIG. 15. Residuals for the Duffing oscillator example ($\sigma = 0$) for the FJet model (top) and RK2 (bottom). The left and right plots are computed according to Eq. C1. The magnitude of the largest dots are given in Table VII.

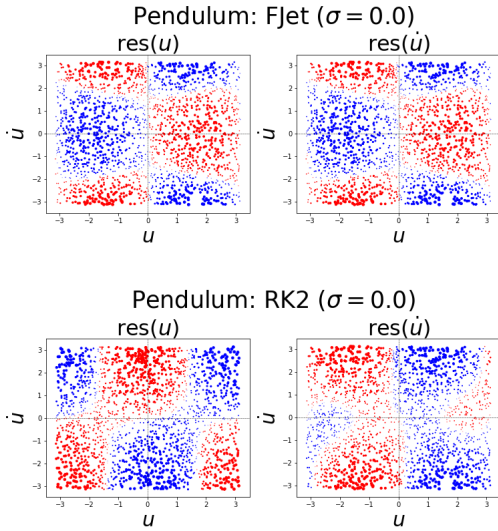


FIG. 14. Residuals for the pendulum example for the FJet model (top) and RK2 (bottom). The left and right plots are computed according to Eq. C1. The magnitude of the largest dots are given in Table VII.

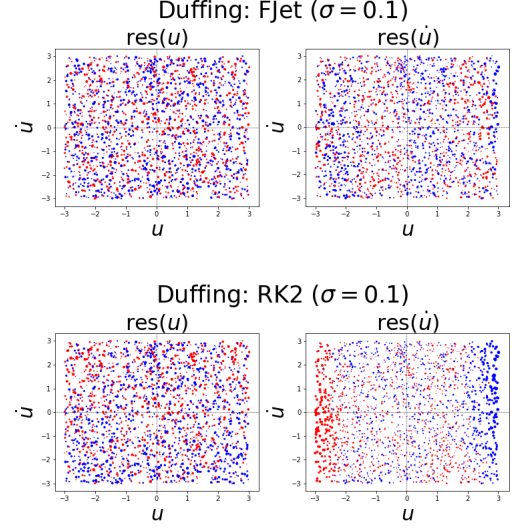


FIG. 16. Residuals for the Duffing oscillator example ($\sigma = 0.1$) for the FJet model (top) and RK2 (bottom). The left and right plots are computed according to Eq. C1. The magnitude of the largest dots are given in Table VII.

Appendix D: Second Optimization

Taking a step back, the building of the model h in Step #3 involved an optimization: minimizing the errors of the data with respect to Δu , $\Delta \dot{u}$ by sampling over different values of u , \dot{u} . However, having done that, it is

possible to perform a second optimization, one in which the parameters are adjusted in order to minimize the error between a single, generated orbit and a corresponding orbit from data. The cost function for this

$$\sum_T \left\{ [u_d(t) - \hat{u}(t)]^2 + \alpha [\dot{u}_d(t) - \hat{\dot{u}}(t)]^2 \right\} \quad (\text{D1})$$

where (u_d, \dot{u}_d) represents the data, $(\hat{u}, \hat{\dot{u}})$ represents the solution generated from the model h , and T signifies the set of times where the data is defined. Note that it is not required that the data be over regular time intervals. The reason this can lead to improvement is that the initial model fitting was premised on finding the best fit for a large set of possible values of u, \dot{u} . This second optimization is instead focused more specifically on the errors near a particular orbit. Note that the choice of $\alpha = 1$ is appropriate to minimize the error in the energy, while $\alpha = 0$ minimizes the error on in u . On a more practical note, the above cost function will be used with greedy updates formed from gaussian perturbations of the parameter values. Finally, as a general consideration, it may be advantageous to include up to the $(n-1)$ st derivative when the underlying ODE is order n .

TABLE VII. This displays the *maximum* magnitudes of the residuals for the FJet and RK2 schemes, where $\text{mx}(u) = \max|\text{res}(u)|$ and likewise for \dot{u} ; the maximum is taken over the data sample. The first three examples use $\sigma = 0$, while the last one uses $\sigma = 0.1$. All values were rounded and multiplied by 10^4 to improve readability.

Example	FJet		RK2	
	$\text{mx}(u)$	$\text{mx}(\dot{u})$	$\text{mx}(u)$	$\text{mx}(\dot{u})$
Harmonic Osc.	3.9×10^{-11}	3.1×10^{-11}	3.9	4.4
Pendulum	0.3	10.8	5.4	16.4
Duffing	5	201	146	1069
Duffing (0.1)	471	855	475	1625

- [1] M. F. Zimmer, arXiv preprint [arXiv:2110.06917](https://arxiv.org/abs/2110.06917) (2021).
- [2] H. Goldstein, *Classical Mechanics*, 2nd ed. (Addison-Wesley, 1980).
- [3] C. R. Galley, Physical Review Letters **110** (2013).
- [4] H. Poincaré, *New Methods of Celestial Mechanics, 1: Periodic and Asymptotic Solutions* (Ed. D.L. Goff) (American Institute of Physics, 1993).
- [5] P. Holmes, Physics Reports **193**, 137 (1990).
- [6] H. Poincaré, J. de Math. **7**, 375 (1881).
- [7] A. M. Lyapunov, *General Problem on Stability of Motion (English translation)* (London, 1992) (Original work published 1892).
- [8] E. A. Jackson, *Perspectives of nonlinear dynamics*, Vol. 1 (Cambridge University Press, 1991).
- [9] J. C. Sprott, *Chaos and Time-Series Analysis* (Oxford, 2003).
- [10] E. N. Lorenz, Journal of Atmospheric Sciences **20**, 130 (1963).
- [11] R. L. Devaney, *An Introduction to Chaotic Dynamical Systems* (Benjamin/Cummings, 1986).
- [12] E. A. Jackson, *Perspectives of nonlinear dynamics*, Vol. 2 (Cambridge University Press, 1991).
- [13] K. Geist, U. Parlitz, and W. L. Born, Progress of Theoretical Physics **83** (1990).
- [14] J. P. Crutchfield and B. S. McNamara, Complex Systems **1**, 417 (1987).
- [15] R. Bowen, CBMS Regional Conference Series in Math. **35** (1978).
- [16] J. Guckenheimer and P. Holmes, *Nonlinear Oscillations, Dynamical Systems, and Bifurcations of Vector Fields* (Springer-Verlag, 1983).
- [17] J. L. McCauley and J. I. Palmore, Physics Letters A **15**, 433 (1986).
- [18] J. I. Palmore and J. L. McCauley, Physics Letters A **122**, 399 (1987).
- [19] C. Grebogi, S. M. Hammel, J. A. Yorke, and T. Sauer, Phys. Rev. Lett. **65** (1990).
- [20] T. Sauer, C. Grebogi, and J. A. Yorke, Phys. Rev. Lett. **79** (1997).
- [21] D. Ruelle and F. Takens, Comm. Math. Phys. **20** (1971).
- [22] N. H. Packard, J. P. Crutchfield, J. D. Farmer, and R. S. Shaw, Physical Review Letters **45** (1980).
- [23] F. Takens, in *Lecture Notes in Mathematics: Dynamical Systems and Turbulence, Warwick 1980 (Coventry, 1979/1980)*, Vol. 898 (Springer, 1981) pp. 366–381.
- [24] J. D. Farmer and J. J. Sidorowich, Physical Review Letters **59**, 845 (1987).
- [25] J. C. Roux, A. Rossi, S. Bachelart, and C. Vidal, Phys. Lett. A **77**, 391 (1980).
- [26] A. Brandstater, J. Swift, H. L. Swinney, A. Wolf, J. D. Farmer, E. Jen, and J. P. Crutchfield, Phys. Lett. A **77**, 391 (1980).
- [27] D. S. Broomhead and D. Lowe, Complex Systems **2**, 321 (1988).
- [28] M. Casdagli, Physica D **35**, 335 (1989).
- [29] J. Cremers and A. Hübler, Zeitschrift für Naturforschung A **42**, 797 (1987).
- [30] J. L. Breeden and A. Hübler, Physical Review A **42** (1990).
- [31] G. Gouesbet, Physical Review A **43**, 5321 (1991).
- [32] G. Gouesbet, Physical Review A **46**, 1784–1796 (1992).
- [33] D. S. Broomhead, R. Indik, A. C. Newell, and D. A. Rand, Nonlinearity **4** (1991).
- [34] L. A. Aguirre and C. Letellier, Mathematical Problems in Engineering **2009** (2009).
- [35] S. Greydanus, M. Dzamba, and J. Yosinski, in *Neural Information Processing Systems (NeurIPS)* (2019) pp. 15353–15363.
- [36] R. Bondesan and A. Lamacraft, arXiv preprint [arXiv:1906.04645](https://arxiv.org/abs/1906.04645) (2019), (Presented at ICML 2019 Workshop on Theoretical Physics for Deep Learning.).
- [37] P. Toth, D. J. Rezende, A. Jaegle, S. Racanière, A. Botev, and I. Higgins (2019).
- [38] M. Lutter, C. Ritter, and J. Peters, in *International Conference on Learning Representations (ICLR)* (2019).
- [39] M. Cranmer, S. Greydanus, S. Hoyer, P. Battaglia, D. Spergel, and S. Ho, in *ICLR 2020 Workshop on Integration of Deep Neural Models and Differential Equations* (2020).
- [40] M. Cranmer, A. Sanchez-Gonzalez, P. Battaglia, R. Xu, K. Cranmer, D. Spergel, and S. Ho, in *Advances in Neural Information Processing Systems 33 (NeurIPS)* (2020).

- [41] S.-M. Udrescu, A. Tan, J. Feng, O. Neto, T. Wu, and M. Tegmark, in *Proc. 34th Conference on Neural Information Processing Systems (NeurIPS)* (Vancouver, Canada, 2020).
- [42] S. H. Rudy, S. L. Brunton, J. L. Proctor, and J. N. Kutz, *Science Advances* **3** (2017).
- [43] R. T. Q. Chen, Y. Rubanova, J. Bettencourt, and D. Duvenaud, in *Neural Information Processing Systems (NeurIPS)* (2018) pp. 6572–6583.
- [44] K. Ott, P. Katiyar, P. Hennig, and M. Tiemann, in *International Conference on Learning Representations (ICLR)* (2021).
- [45] P. Kidger, arXiv preprint [arXiv:2202.02435](https://arxiv.org/abs/2202.02435) (2022).
- [46] G. E. P. Box, G. M. Jenkins, G. C. Reinsel, and G. M. Ljung, *Time Series Analysis: Forecasting and Control*, 5th ed. (Wiley, 2015).
- [47] E. Hairer, S. P. Nørsett, and G. Wanner, *Solving Ordinary Differential Equations I – Nonstiff Problems* (Springer, 1987).
- [48] W. H. Press, S. A. Teukolsky, W. T. Vetterling, and B. P. Flannery, *Numerical Recipes, The Art of Scientific Computing*, 3rd ed. (Cambridge University Press, 2007).
- [49] M. Schober, D. Duvenaud, and P. Hennig, in *Neural Information Processing Systems (NeurIPS)* (2014).
- [50] P. J. Olver, *Applications of Lie Groups to Differential Equations*, 2nd ed. (Springer-Verlag, 1993).
- [51] I. Knowles and R. J. Renka, *Electronic Journal of Differential Equations, Conference* **21**, 235–246 (2014).
- [52] C. Letellier, L. A. Aguirre, and U. S. Freitas, *Chaos* **19** (2009).
- [53] N. Wiener, *Bull. Amer. Math. Soc.* **56**, 378–381 (1950).
- [54] T. Hastie, R. Tibshirani, and J. Friedman, *The Elements of Statistical Learning: Data Mining, Inference, and Prediction*, 2nd ed. (Springer-Verlag, 2009).
- [55] A. P. Young, “Physics 115/242, Comparison of methods for integrating the simple harmonic oscillator,” (2020).
- [56] G. Duffing, *Vieweg, Braunschweig* **41/42** (1918).
- [57] P. J. Holmes and D. A. Rand, *Journal of Sound and Vibration* **44**, 237 (1976).
- [58] F. C. Moon and P. J. Holmes, *Journal of Sound and Vibration* **65**, 275 (1979).
- [59] D. W. Jordan and P. Smith, *Nonlinear ordinary differential equations – An introduction for scientists and engineers*, 4th ed. (Oxford University Press, 2007).
- [60] O. Menard, C. Letellier, J. Maquet, L. L. Sceller, and G. Gouesbet, *International Journal of Bifurcation and Chaos* **10**, 1759–1772 (2000).